Article

Intrinsic Primary and Secondary Hydrogen Kinetic Isotope Effects for Alanine Racemase from Global Analysis of Progress Curves

M. Ashley Spies, and Michael D. Toney

J. Am. Chem. Soc., **2007**, 129 (35), 10678-10685• DOI: 10.1021/ja067643k • Publication Date (Web): 10 August 2007

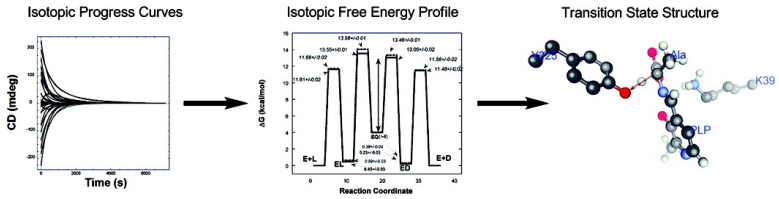

More About This Article

Additional resources and features associated with this article are available within the HTML version:

- Supporting Information
- Links to the 2 articles that cite this article, as of the time of this article download
- Access to high resolution figures
- Links to articles and content related to this article
- Copyright permission to reproduce figures and/or text from this article

View the Full Text HTML

J|A|C|S
ARTICLES
Published on Web 08/10/2007

Intrinsic Primary and Secondary Hydrogen Kinetic Isotope Effects for Alanine Racemase from Global Analysis of Progress Curves

M. Ashley Spies[†] and Michael D. Toney*[,‡]

Contribution from the Department of Biochemistry, University of Illinois, Urbana, Illinois 61801, and Department of Chemistry, University of California, One Shields Avenue, Davis, California 95616

Received October 25, 2006; E-mail: mdtoney@ucdavis.edu

Abstract: The pyridoxal phosphate dependent alanine racemase catalyzes the interconversion of L- and D-alanine. The latter is an essential component of peptidoglycan in cell walls of Gram-negative and -positive bacteria, making alanine racemase an attractive target for antibacterials. Global analysis of protiated and deuterated progress curves simultaneously enables determination of intrinsic kinetic and equilibrium isotope effects for alanine racemase. The intrinsic primary kinetic isotope effects for Cα hydron abstraction are 1.57 ± 0.05 in the D → L direction and 1.66 ± 0.09 in the L → D direction. Secondary kinetic isotope effects were found for the external aldimine formation steps in both the L → D (1.13 ± 0.05, forward; 0.90 ± 0.03, reverse) and D → L (1.13 ± 0.06, forward; 0.89 ± 0.03, reverse) directions. The secondary equilibrium isotope effects calculated from these are 1.26 ± 0.07 and 1.27 ± 0.07 for the L → D and D → L directions, respectively. These equilibrium isotope effects imply substantial ground-state destabilization of the C−H bond via hyperconjugation with the conjugated Schiff base/pyridine ring π system. The magnitudes of the intrinsic primary kinetic isotope effects, the lower boundary on the energy of the quinonoid intermediate, and the protonation states of the active site catalytic acids/bases (K39-ϵNH_2 and Y265-OH) suggest that the pK_a of the substrate Cα−H bond in the external aldimine lies between those of the two catalytic bases, such that the proton abstraction transition state is early in the D → L direction and late in the L → D direction.

Introduction

Alanine racemase (AlaR; E.C. 5.1.1.1) catalyzes the stereoisomerization of alanine. D-Alanine is an essential component of the peptide cross-links in the peptidoglycan layer of bacterial cell walls in both Gram-negative and -positive species.[1] Peptidoglycan cross-linking is essential to survival,[2] making AlaR an attractive antibacterial target.

AlaR utilizes pyridoxal 5′-phosphate (PLP) as an essential cofactor. It possesses a type III PLP fold and is a homodimer, with each monomer composed of a classic α/β barrel plus a second β-strand domain.[3]

A wealth of mechanistic information is available for AlaR.[3−10] It employs a two-base mechanism.[9,10] Site-directed mutagenesis studies have established that Y265 acts as a base in the L → D direction and an acid in the D → L direction,[11] while K39, which forms the internal aldimine with the PLP cofactor, is a base in the D → L direction and an acid in the L → D direction (see Figure 1).[10]

Crystal structures of AlaR show a hydrogen bond between a fully conserved arginine (R219 in *Bacillus stearothermophilus*) and the pyridine nitrogen.[3,7,8,12] This interaction precludes protonation of the pyridine nitrogen given the pK_a differences between these functional groups, thereby preventing full implementation of the "electron sink" potential of the pyridine ring. This suggests that if a carbanionic ("quinonoid") intermediate exists, it is not stabilized to the fullest possible extent. In fact, no quinonoid intermediate is spectroscopically detectable with wild-type *B. stearothermophilus* AlaR,[6] but the R219E mutant does show buildup of the quinonoid intermediate.[9]

The absence of an observable quinonoid intermediate in wild-type AlaR begged the question of whether stereoinversion occurs through a concerted double proton transfer, avoiding this intermediate. Therefore, a precise method for determining multiple hydrogen kinetic isotope effects (KIEs)[5] that is a modification of the equilibrium perturbation[13] and washout[14]

[†] University of Illinois.
[‡] University of California.

(1) Neidhart, F. C. *Escherichia coli and Salmonella*, 2nd ed.; Blackwell Publishing: London, 1999.
(2) Walsh, C. T. *J. Biol. Chem.* **1989**, *264*, (5), 2393−6.
(3) Shaw, J. P.; Petsko, G. A.; Ringe, D. *Biochemistry* **1997**, *36*, 1329−1342.
(4) Faraci, W. S.; Walsh, C. T. *Biochemistry* **1988**, *27*, 3267−76.
(5) Spies, M. A.; Toney, M. D. *Biochemistry* **2003**, *42*, 5099−107.
(6) Spies, M. A.; Woodward, J. J.; Watnik, M. R.; Toney, M. D. *J. Am. Chem. Soc.* **2004**, *126*, 7464−75.
(7) Stamper, C. G. F.; Morollo, A. A.; Ringe, D. *Biochemistry* **1998**, *37*, 10438−10445.
(8) Stamper, G. F.; Morollo, A. A.; Ringe, D. *Biochemistry* **1999**, *38*, 6714.
(9) Sun, S. X.; Toney, M. D. *Biochemistry* **1999**, *38*, 4058−4065.
(10) Watababe, A.; Kurokawa, Y.; Yoshimura, T.; Kurihara, T.; Soda, K.; Esaki, N. *J. Biol. Chem.* **1999**, *274*, 4189−4194.
(11) Watanabe, A.; Kurokawa, Y.; Yoshimura, T.; Esaki, N. *J. Biochem.* **1999**, *125*, 987−990.
(12) Watanabe, A.; Yoshimura, T.; Mikami, B.; Hayashi, H.; Kagamiyama, H.; Esaki, N. *J. Biol. Chem.* **2002**, *277*, 19166−72.
(13) Schimerlik, M. I.; Rife, J. E.; Cleland, W. W. *Biochemistry* **1975**, *14*, 5347−54.

10.1021/ja067643k CCC: $37.00

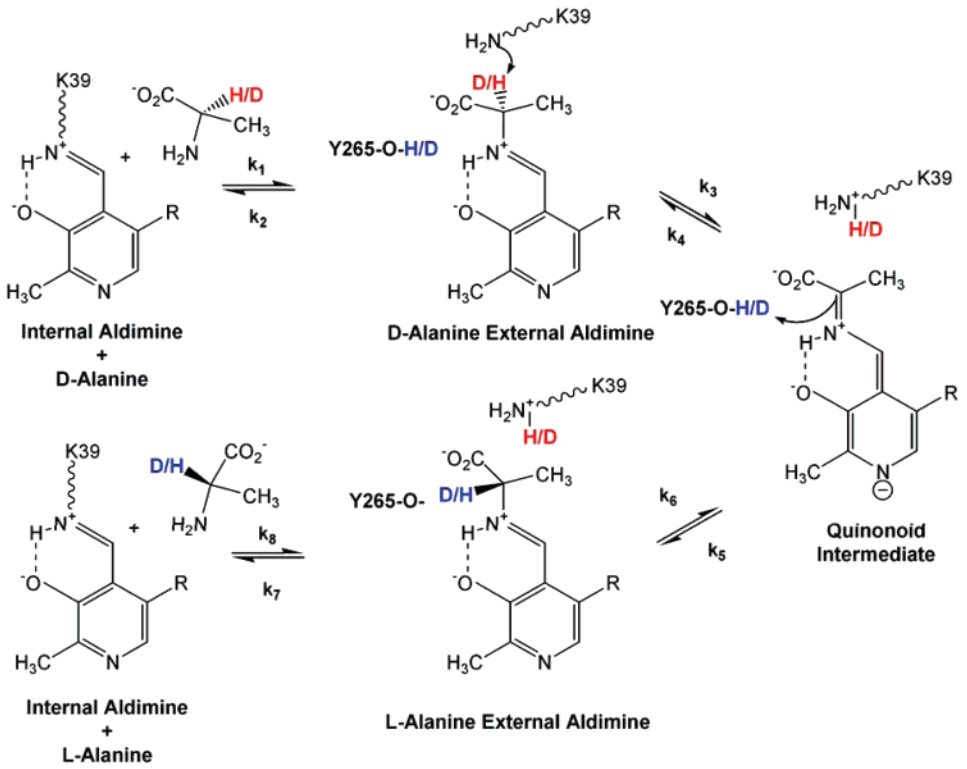

Figure 1. Mechanism of AlaR. The reaction shown is from D-alanine → L-alanine. Lys39 is covalently bound to the PLP cofactor ("internal aldimine") and is displaced via nucleophilic attack by the α-amino group of D-alanine to yield the "external aldimine". Hydron abstraction by Lys39 produces a quinonoid intermediate, which is reprotonated from the opposite face by Tyr265 to yield the external aldimine of L-alanine. Re-formation of the internal aldimine releases L-alanine. The Cα proton of D-alanine (red) is transferred to Lys39 and the Cα proton of L-alanine (blue) is transferred to Tyr265. Both are irreversibly washed out into the solvent.

techniques was developed to address this question. Its application confirmed the stepwise nature of the mechanism. Recent computational work from Gao's group also confirmed the existence of the quinonoid intermediate and its high energy relative to the external aldimine intermediates.[15,16]

Figure 1 summarizes the fate of the substrate Cα hydron in AlaR. The hydron of the external aldimine of D-alanine (red) is abstracted by Lys39 and subsequently lost to solvent. The quinonoid intermediate is reprotonated at the opposite face with a solvent-derived hydron from Tyr265 (blue), giving the external aldimine of L-alanine. Schiff base interchange with Lys39 regenerates the internal aldimine and releases L-alanine with a solvent-derived Cα hydron.

Free energy profiles for AlaR at two pH values were recently determined by global nonlinear least-squares analysis of racemization progress curves[6] using the program DynaFit.[17] The free energy profiles determined in that study were consistent with a number of experimental observations such as steady-state kinetic parameters, viscosity effects, equilibrium overshoots in D_2O, and the lower energy boundary of the quinonoid intermediate.

The more ambitious goal of this work is to apply global analysis to isotopic progress curves. The resulting isotopic free energy profiles could be used to determine *intrinsic* KIEs directly, as opposed to calculating them using commitment factors.[6] The mechanism in Figure 1 allows for two primary and four secondary KIEs. The latter can be used to calculate two secondary equilibrium isotope effects (EIEs). The primary KIEs occur in Cα proton abstraction, while the secondary effects are due to hyperconjugation of the Cα−H bond with the conjugated Schiff base/pyridine ring π system in the external aldimine intermediate.

Intrinsic KIEs are widely regarded as the best tool for probing the structure of transition states of chemical reactions.[18,19] Their power and utility when coupled to computational chemistry has been demonstrated by Schramm and co-workers in the development of tight-binding transition-state analogues to purine nucleoside phosphorylase, for example.[20−22] This type of application has been limited partly due to the experimental difficulties in obtaining the required KIEs. Global analysis of isotopic progress curves is an attractive alternative to classical KIE measurements for obtaining intrinsic KIEs for transition-state analysis.

The introduction of isotopes significantly complicates global analysis of progress curves. The coupled isotopic washout and racemization manifolds involved in the AlaR mechanism are shown in Scheme 1. The complete reaction scheme consists of 18 rate constants and allows for differences in the rate constants for binding and release of the isotopic alanines. A simplified version is shown in Scheme 2, which has 14 rate constants and does not allow for isotope effects on external aldimine formation. It is demonstrated here that the 18-parameter model gives

(14) Bahnson, B. J.; Anderson, V. E. *Biochemistry* **1991**, *30*, 5894−906.
(15) Major, D. T.; Gao, J. *J. Am. Chem. Soc.* **2006**, *128*, 16345−57.
(16) Major, D. T.; Nam, K.; Gao, J. *J. Am. Chem. Soc.* **2006**, *128*, 8114−5.
(17) Kuzmic, P. *Anal. Biochem.* **1996**, *237*, 260−73.
(18) Cleland, W. W.; O'Leary, M. H.; Northrop, D. B. *Isotope Effects on Enzyme-Catalyzed Reactions*; University Park Press: Baltimore, 1977.
(19) Northrop, D. B. *Annu. Rev. Biochem.* **1981**, *50*, 103−31.
(20) Kline, P. C.; Schramm, V. L. *Biochemistry* **1993**, *32*, 13212−9.
(21) Miles, R. W.; Tyler, P. C.; Furneaux, R. H.; Bagdassarian, C. K.; Schramm, V. L. *Biochemistry* **1998**, *37*, 8615−21.
(22) Schramm, V. L. *Acc. Chem. Res.* **2003**, *36*, 588−96.

Scheme 1

18 Parameter Deuterium Washout Model

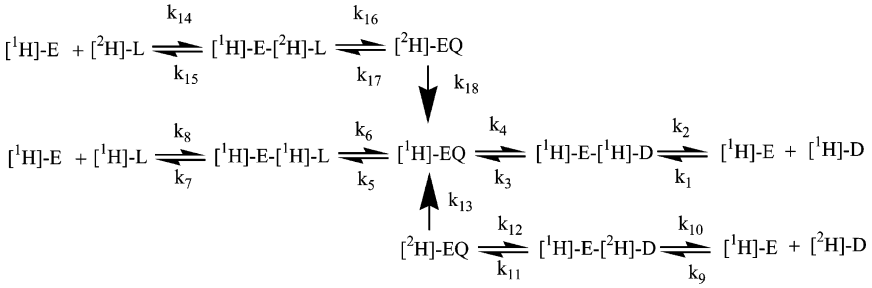

Scheme 2

14 Parameter Deuterium Washout Model

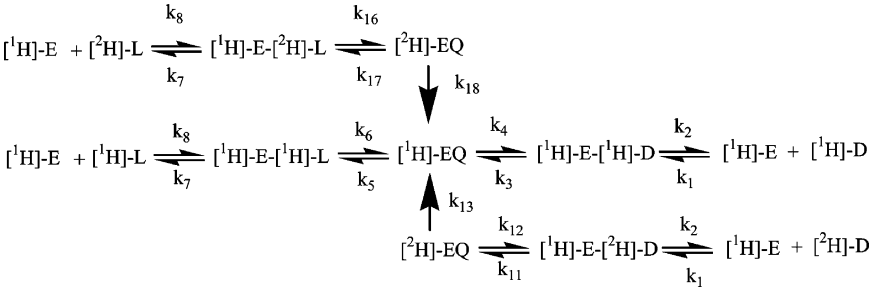

a statistically significant better fit to the data. Thus, intrinsic secondary KIEs on external aldimine formation, and thereby secondary EIEs on this same step, are obtained.

Herein, equilibrium perturbation, isotopic washout, and racemization progress curves are used to constrain the search for rate constants that best describe the three manifolds of Scheme 1. The intrinsic primary KIEs, and secondary KIEs and EIEs, obtained provide insight into the nature of proton abstraction from Cα for the two stereoisomers of the external aldimine intermediate. The results suggest that the Cα−H pK_a in the external aldimine lies between the microscopic pK_a values of the two catalytic bases and that labilization of this bond occurs through both ground- and transition-state effects.

Experimental Section

Materials. D- and L-alanine were purchased from Aldrich (99% pure). Buffers were from Fisher. *B. stearothermophilus* AlaR was prepared as described previously.[9] Deuterated D-alanine was purchased from CDN Isotopes (Quebec, Canada; catalog number D-1274, 98 atom %). Deuterated L-alanine was purchased from Isotech, Inc.

Progress Curves. A Jasco 720 circular dichroism spectrophotometer was used for all experiments. The wavelength (215 nm) was selected so that the CD signal and PMT voltage were linear with amino acid concentration. Initial D- and L-alanine concentrations were varied from 0.1 to 20 mM (0.05K_M to 10K_M). The buffer was 50 mM potassium borate, pH 8.48, with 100 mM potassium chloride. The temperature was maintained at 25 °C with a circulating water bath. The enzyme concentration varied from 5 to 26 nM.

Computational Procedures. See the Supporting Information.

Results

All-Protiated Manifold ($k_1 \rightarrow k_8$). The central manifold in Schemes 1 and 2 consists of simple racemization of protiated substrates in water. This is the same system analyzed by Spies et al.[6] Here, a new set of progress curves for racemization of protiated substrates in H_2O was acquired at pH 8.48 (vs pH 8.9 in the previous study). Optimization of rate constants k_1-k_8 following the previous procedures produced results very similar to those obtained in the previous study (Table S1 in the Supporting Information). Here, the final free energy profile for the all-protiated system ($k_1 \rightarrow k_8$) was constructed from rate constants obtained from fitting the 18-parameter model to all available data (see below).

Optimization of Primary KIEs with the 14-Parameter Model. The rate constants from the all-protiated analysis were used as initial estimates for fitting isotopic progress curves to the 14-parameter model (Scheme 2). Fitting to a random selection of racemization and washout progress curves was employed. Tables S1−S3 (Supporting Information) give rate constants and primary KIEs and compare the intrinsic KIEs to the corresponding values calculated using commitments to catalysis and experimental KIEs.[6]

Optimization of Rate Constants in the 18- and 14-Parameter Models. Unlike the 14-parameter model, the 18-parameter model allows for isotopic differences in the rate constants for external aldimine formation. The initial estimates for the rate constants of the 18-parameter model were the fitted values from the previous step (i.e., optimization of the 14-parameter model). Additionally, randomization of the rate constants for external aldimine formation by ±10% was performed to allow for secondary KIEs. Again, random selection of and fitting to racemization and washout progress curves was employed.

Figure 2A shows a representative fit (of 45 total). A similar optimization (30 fits total) in which substrate binding and release rate constants were randomized by ±10% was carried out using the 14-parameter model. Table S2 shows that the primary KIEs (k_3/k_{11} and k_6/k_{16}) for the two sets of fits are similar, with the 14-parameter model yielding somewhat larger primary KIEs. The important difference is the larger errors on the KIEs (due to errors on k_{11} and k_{16}) in the 14-parameter model.

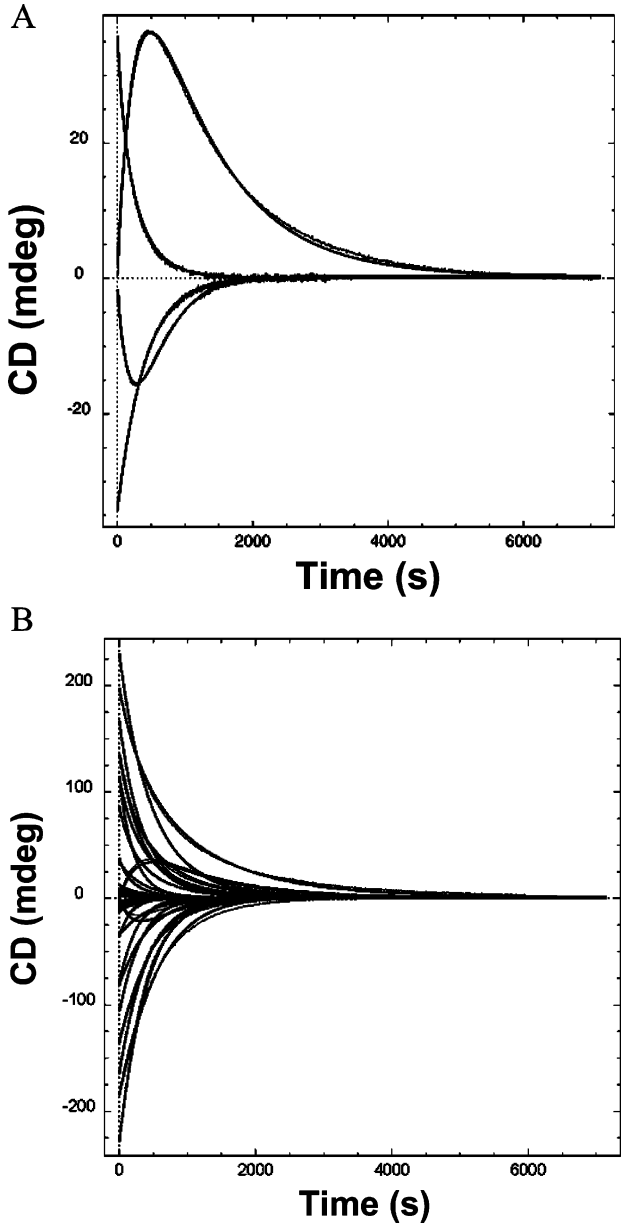

Figure 2. Representative fits to the 18-parameter model. (A) Fit where two equilibrium perturbations and a random selection of two (one D and one L) racemization progress curves were employed. The entire analysis contituted 45 such fits. (B) Fit where all available data (racemizations, washouts, and equilibrium perturbations) were employed.

Strikingly, the 18-parameter model shows a strong preference for a normal secondary KIE on Schiff base formation for both D-Ala (k_1/k_9) and L-Ala (k_8/k_{14}). Plots of the mean square for a given fit versus the corresponding calculated secondary KIE for the forward reaction E + Ala → ES for D-Ala → L-Ala and the reverse reaction ES → E + Ala for D-Ala → L-Ala are presented in Figure S1A,B (see the Supporting Information), respectively. The lower boundary for the forward reaction (sp^3 → sp^2-like, due to weakening of the Cα−H bond by hyperconjugation) is a KIE of unity, which is the upper boundary for the reverse reaction (sp^2-like → sp^3). The average values for the secondary KIEs and their standard deviations are shown in Table S2. Table 1 shows the fitted rate constants ("averaged") for the 18-parameter model using this procedure. Table S4 (Supporting Information) gives the fitted rate constants for the 14-parameter model using this procedure.

Final Refinement of the Rate Constants in the 18-Parameter Model. Additional refinement was achieved by randomizing all rate constants from the 18-parameter model fit described above (i.e., "averaged" rate constant set, Table 1) followed by refitting and averaging them over these fits.

Two approaches were taken. The first was fitting to a random sample of progress curves as employed in the previous steps. The second involved fitting the entire pool of progress curves (racemizations, washouts, and equilibrium perturbations, 39 total, representative fit shown in Figure 2B). The latter method was prohibited in the early phases of the refinement procedure by poor initial estimates that resulted in lack of convergence errors. Table 1 compares the results of the three procedures used here to estimate the rate constants for the 18-parameter model.

Table 2 provides a comparison of the calculated intrinsic KIE and mean square values for the two final refinement methods. Both produce rate constants and KIEs that are similar. A notable difference, however, is in the value of the intrinsic primary KIE in the D → L (k_3/k_{11}) direction, which is significantly larger when all progress curves are included in each fit. Also, the large scatter in secondary KIEs seen using random selection of progress curves (Figure S1A,B, Supporting Information) is significantly reduced when all progress curves are included in each fit (Figure S1C,D). The free energy profiles in Figure 3 were constructed from the rate constants for the 18-parameter model refined by including all progress curves in each fit.

Fitting the 18-parameter model to all progress curves produced a lower mean square (1.49) than a similar fit to all progress curves using the 14-parameter model (2.12). The statistical significance of this difference was determined using an *F*-test. The *F*-statistic (=1.42, here) is the quotient of the mean square values for the comprehensive fits to the 14- and 18-parameter models, respectively.

To estimate the number of "observations" that may be ascribed to any given progress curve, individual progress curves were fitted to a simple one-substrate, one-intermediate, one-product reversible racemization mechanism. All four steady-state kinetic parameters (i.e., forward and reverse k_{cat} and K_M values) were well determined by these fits to single progress curves (see Supporting Information Table S6). Therefore, each progress curve is conservatively counted as four independent observations here. The degrees of freedom are calculated by subtracting the number of parameters (i.e., 14 or 18) from the number of observations. This gives 142 degrees of freedom for the 14-parameter model (Scheme 2) and 138 degrees of freedom for the 18-parameter model (Scheme 1). The *p* value (probability that additional parameters in the larger model are not warranted) is 0.02. Thus, there is a ~98% chance that the secondary KIEs on Schiff base interchange reported here are statistically significant.

Secondary Equilibrium Isotope Effects from ab Initio Calculations. Supporting Information Table S5 compares calculated EIEs for two test cases where experimental secondary EIEs are known and gives EIEs for three prototropic isomers of the PLP/alanine aldimine. The calculated EIEs are ~90% of the experimental values for the test cases. The results for the three aldimine prototropic isomers confirm there is a secondary EIE, but these are smaller than the experimental values found

Table 1. Rate Constants for the 18-Parameter Model

	averaged[a]	error (%)	optimized, averaged[b]	error (%)	optimized, all data[c]	error (%)
k_1 ($M^{-1}\,s^{-1}$)	$(2.356 \pm 0.008) \times 10^7$	0.3	$(2.37 \pm 0.08) \times 10^7$	3.4	$(2.35 \pm 0.07) \times 10^7$	3.2
k_2 (s^{-1})	$(3.439 \pm 0.007) \times 10^4$	0.2	$(3.44 \pm 0.09) \times 10^4$	2.6	$(3.48 \pm 0.08) \times 10^4$	2.4
k_3 (s^{-1})	$(2.41 \pm 0.02) \times 10^3$	0.8	$(2.41 \pm 0.07) \times 10^3$	2.9	$(2.48 \pm 0.06) \times 10^3$	2.5
k_4 (s^{-1})	$(5.84 \pm 0.1) \times 10^9$	2.3	$(5.89 \pm 0.19) \times 10^9$	3.2	$(5.82 \pm 0.17) \times 10^9$	5.8
k_5 (s^{-1})	$(2.49 \pm 0.1) \times 10^9$	4.2	$(2.49 \pm 0.07) \times 10^9$	2.8	$(2.53 \pm 0.06) \times 10^9$	2.4
k_6 (s^{-1})	$(1.56 \pm 0.02) \times 10^3$	1.3	$(1.54 \pm 0.05) \times 10^3$	3.2	$(1.55 \pm 0.03) \times 10^3$	1.7
k_7 (s^{-1})	$(4.09 \pm 0.02) \times 10^4$	0.5	$(4.10 \pm 0.09) \times 10^4$	2.2	$(4.05 \pm 0.07) \times 10^4$	1.8
k_8 ($M^{-1}\,s^{-1}$)	$(1.847 \pm 0.004) \times 10^7$	0.2	$(1.867 \pm 0.05) \times 10^7$	2.9	$(1.89 \pm 0.06) \times 10^7$	2.9
k_9 ($M^{-1}\,s^{-1}$)	$(2.2 \pm 0.2) \times 10^7$	9.1	$(2.1 \pm 0.2) \times 10^7$	9.5	$(2.08 \pm 0.07) \times 10^7$	3.7
k_{10} (s^{-1})	$(3.8 \pm 0.4) \times 10^4$	11	$(4.0 \pm 0.5) \times 10^4$	11.4	$(3.9 \pm 0.09) \times 10^4$	2.4
k_{11} (s^{-1})	$(1.7 \pm 0.3) \times 10^3$	18	$(1.9 \pm 0.3) \times 10^3$	14.8	$(1.6 \pm 0.04) \times 10^3$	2.4
k_{12} (s^{-1})	$(2 \pm 6) \times 10^9$	300	$(2 \pm 9) \times 10^9$	450	$(2.3 \pm 0.2) \times 10^9$	6.5
k_{13} (s^{-1})	$>10^{10}$		$>10^{10}$		$>10^{10}$	
k_{14} ($M^{-1}\,s^{-1}$)	$(1.62 \pm 0.08) \times 10^7$	5.0	$(1.54 \pm 0.05) \times 10^7$	3.2	$(1.67 \pm 0.05) \times 10^7$	3.0
k_{15} (s^{-1})	$(4.7 \pm 0.3) \times 10^4$	6.4	$(4.9 \pm 0.1) \times 10^4$	2.7	$(4.5 \pm 0.1) \times 10^4$	2.7
k_{16} (s^{-1})	$(9 \pm 1) \times 10^2$	11	$(9.4 \pm 0.7) \times 10^2$	7.4	$(9.3 \pm 0.2) \times 10^2$	2.5
k_{17} (s^{-1})	$>10^{10}$		$>10^{10}$		$>10^{10}$	
k_{18} (s^{-1})	$>10^{10}$		$>10^{10}$		$>10^{10}$	

[a] Averaged from 45 independent fits. Progress curves were selected from a pool of 39 with the stipulation that each global fit contained one for each L- and D-alanine (either [^{2}H]Ala or [^{1}H]Ala). A total of four data files were fitted (i.e., two perturbations and two progress curves). All rate constants were adjustable parameters. Initial values for the rate constants were from optimization with the 14-parameter model, except that association (k_9, k_{14}) and dissociation (k_{10}, k_{15}) rate constants for deuterated alanine were randomized by ±10%. [b] Averaged from 20 independent fits. Rate constants from the "averaged" set were randomized by 5% and refitted using random selection of four curves for fitting. The fitted rate constants and mean square values were averaged and the standard deviation was determined for each rate constant. All rate constants were adjustable parameters. [c] Averaged from 20 independent fits. Rate constants from the "averaged" set were randomized by 5% and globally fitted to the complete set of data. All rate constants were adjustable parameters.

Table 2. Isotope Effects for the 18-Parameter Model

	two equilibrium perturbations plus two racemization progress curves[a]	all data simultaneously[b]
average mean square deviation	0.3 ± 0.3	1.49 ± 0.06
primary KIE, D → L	1.25 ± 0.19	1.57 ± 0.05
primary KIE, L → D	1.64 ± 0.14	1.66 ± 0.09
secondary KIE, D → L (forward)	1.15 ± 0.13	1.13 ± 0.06
secondary KIE, D → L (reverse)	0.86 ± 0.10	0.89 ± 0.03
secondary KIE, L → D (forward)	1.21 ± 0.05	1.13 ± 0.05
secondary KIE, L → D (reverse)	0.84 ± 0.03	0.90 ± 0.03
K_H/K_D, D → L[c]	1.34 ± 0.22	1.27 ± 0.07
K_H/K_D, L → D[c]	1.44 ± 0.09	1.26 ± 0.07

[a] Rate constants from the "averaged" set were randomized by 5% and 20 sets refitted. All rate constants were adjustable parameters. [b] Rate constants from the "optimized, averaged" set were randomized by 5% and globally fitted to the complete set of data. All rate constants were adjustable parameters. [c] The equilibrium constants are calculated as association constants.

here. The Cα−H/D bond was fixed parallel to the Schiff base π bond in these calculations.

Discussion

Refinement Process. Recently, global analysis of racemization progress curves was shown to give all-protiated free energy profiles for AlaR.[6] In principle, progress curves for both Cα-protiated and -deuterated alanine combined in a single global analysis should have enough information to define the free energy profiles for both isotopes and thereby the intrinsic KIEs. However, the isotopic manifolds add a significant degree of complexity to the simpler all-protiated system, necessitating the use of bootstrap methods to obtain convergent global fits.

Here, sets of progress curves for Cα-protiated and -deuterated L- and D-alanine were incrementally fitted to models of increasing complexity. Initially, the all-protiated manifold was optimized, which gave rate constants very similar to those obtained previously from an independent set of progress curves collected at a higher pH (8.9 previously vs 8.48 here).[6] Next, the eight rate constants obtained from the all-protiated optimization were employed as initial estimates for the 14-parameter model, the results of which were then employed as initial estimates for the 18-parameter model.

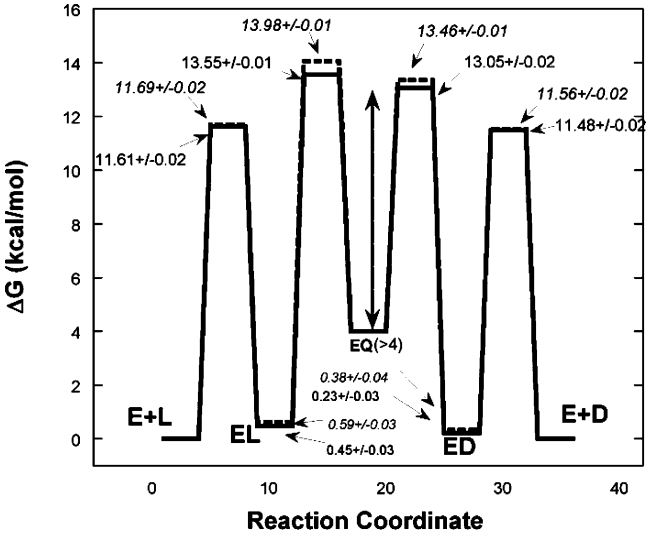

Figure 3. Free energy profiles from fits of the 18-parameter model to all available data. The standard state is 1 mM alanine. The solid line is for protiated substrates, while the dashed line is for deuterated substrates. The double arrow represents the region of uncertainty for the quinonoid intermediate.[6] Energy values and their errors are indicated for each state.

Once rate constants that yielded simulated progress curves close to the experimental data were obtained, final refinement by rate constant randomization and refitting to all data sets simultaneously was possible. A similar refinement using the random sampling strategy employed in previous steps produced similar but less precise results.

Reverse Protonation in AlaR Catalysis. A large number of enzymes employ a combination of general-acid/base catalysts where differently protonated forms of the enzyme occur at the beginning and end of the reaction.[23] For a two-base mechanism, such as that catalyzed by AlaR, there are four possible

protonation states: (**1**) K39-NH_3^+/Y265-OH, (**2**) K39-NH_3^+/Y265-O^-, (**3**) K39-NH_2/Y265-OH, and (**4**) K39-NH_2/Y265-O^-. Protonation states **2** and **3** both have the same number of protons, but **2** should predominate on the basis of pK_a values of ~7.4 assigned to Y265 and >10 assigned to K39.[9]

This is similar to the interconversion of 2-phospho-D-glycerate (2-PGA) and phosphoenol pyruvate (PEP) catalyzed by enolase. Sims et al.[23] disentangled the contributions of the four protonation states (similar to the four shown above) of enolase. They hypothesized that, even when the catalytically active protonation state is present in small quantities at the pH optimum, a catalytic advantage is gained from a high general-base pK_a that is closer to that of the carbon acid. Sims et al. referred to the active protonation state of enolase in the PEP → 2PGA direction as the "typical" one (analogous to **2**) since the pK_a values of the general-acid/base catalysts favor it and to the less populated form (analogous to **3**) as the "reverse" protonation state since the pK_a values of the general-acid/base catalysts disfavor it. A notable conclusion of Sims et al. was that the ratio of the typical to the reverse protonation state is constant across the entire pH range, although each species' concentration changes with pH.

For AlaR, only the macroscopic pK_a values are known, and it is not possible (as Sims et al. were able to do for enolase) to calculate the concentration of the reverse protonation state (**3**) that must be present to catalyze the D → L reaction. There can be large differences between the microscopic and macroscopic pK_a values; thus, it is not unreasonable that K39 of AlaR has a microscopic pK_a of 11 or higher. The likelihood of this is bolstered by the close proximity of the side chain amino group of K39 to the carboxylate of the highly conserved D313. Lysine pK_a values in active sites of enzymes have been shown to be perturbed by several units relative to that of the free amino acid due to their proximity to other charged residues.[24] The proposal that K39 has a pK_a similar to or higher than that of the substrate Cα in the external aldimine intermediate is pertinent to the KIE discussion that follows.

Magnitudes of Primary KIEs. The intrinsic primary hydrogen KIEs determined in this study are small compared to the semiclassical limit. One explanation for the small values is that the transition states are very asymmetric. The KIEs correspond to less than ~10% or greater than ~90% hydron transfer in the transition state in the Westheimer model.[25] Westheimer−Melander theory[25,26] predicts that the magnitude of the intrinsic primary KIE varies with both the extent of transfer in the transition state and the angle (A−H−B) of transfer between the donor and acceptor. This has been demonstrated in the sodium borohydride/deuteride reduction of *para*-substituted benzyl chlorides,[27] where primary hydrogen KIEs as low 1.14 were determined to be due to nonlinear transition states. A second explanation for the small primary KIEs is a large contribution of ground-state quantum mechanical tunneling for both the H and D reactions. Experimental and

Scheme 3

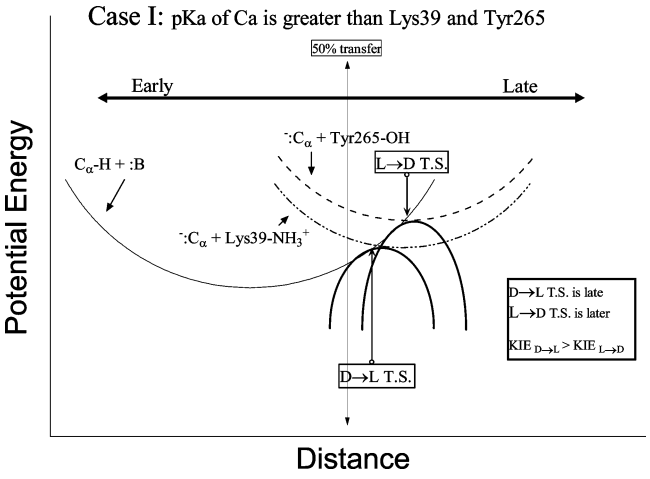

theoretical work on enzyme-catalyzed proton tunneling has elaborated on vibration-driven "extreme tunneling".[28−30]

From recent QM/MM computational studies on AlaR, it was concluded that quantum mechanical tunneling does not contribute significantly to the proton-transfer steps. That work also does not support a nonlinear proton-transfer transition state as the source of the small primary KIEs observed here. Therefore, the following discussion is conservatively based on the simple Westheimer model, which relates the magnitude of a KIE to the extent of hydron transfer in the transition state.

Transition-State Structures for Proton Transfers. The magnitude of the intrinsic primary hydrogen KIEs (k_3/k_{11} and k_6/k_{16}) can be related to the position of the proton in flight in a classical transition state via the Westheimer model in which a KIE is maximal when ΔpK_a between the proton donor and acceptor is zero, with decreasing KIEs on either side of the maximum.[25]

Dixon and Bruice[31] analyzed the general-base-catalyzed racemization of aldimines formed from alanine and 3-hydroxypyridine-4-carboxyaldehyde and estimated the alanine Cα pK_a to range from ~9 to 14, depending on the protonation state of the aldimine. Although the actual pK_a of the aldimine Cα proton in the active site is unknown, it is reasonable to expect that the active site environment is capable of lowering it relative to that in water by several units. The average pK_a for the three protonation states of the alanine/3-hydroxypyridine-4-carboxyaldehyde Schiff base in solution is ~11.5, and a mere 2 unit decrease in this value at the active site could place the substrate pK_a between those of Y265 and K39. Therefore, three scenarios for ΔpK_a values between proton donors and acceptors in the active site can reasonably be considered given the substantially lower pK_a of Y265 compared to K39.[9] Schematic potential energy diagrams illustrate these (Schemes 3−5).

Each curve in Schemes 3−5 represents an idealized energy well for the transferred proton. In each case, the reactant is on the left (Cα proton plus either K39-NH_2 or Y265-O^-) and the products (carbanion plus either K39-NH_3^+ or Y265-OH) are on the right. The crossover points between potential energy

(23) Sims, P. A.; Larsen, T. M.; Poyner, R. R.; Cleland, W. W.; Reed, G. H. *Biochemistry* **2003**, *42*, 8298−306.
(24) Kenyon, G. L.; Gerlt, J. A.; Petsko, G. A.; Kozarich, J. W. *Acc. Chem. Res.* **1995**, *28*, 178−186.
(25) Westheimer, F. H. *Chem. Rev.* **1961**, *1*, 265.
(26) Melander, L. *Isotope Effects on Reaction Rates*; Roland Press: New York, 1960; p 24.
(27) Koerner, T.; Fang, Y.; Westaway, K. C. *J. Am. Chem. Soc.* **2000**, *122*, 7342−7350.
(28) Basran, J.; Sutcliffe, M. J.; Scrutton, N. S. *Biochemistry* **1999**, *38*, 3218−22.
(29) Kohen, A.; Cannio, R.; Bartolucci, S.; Klinman, J. P. *Nature* **1999**, *399*, 496−9.
(30) Scrutton, N. S.; Basran, J.; Sutcliffe, M. J. *Eur. J. Biochem.* **1999**, *264*, 666−71.
(31) Dixon, J. E.; Bruice, T. C. *Biochemistry* **1973**, *12*, 4762−6.

Scheme 4

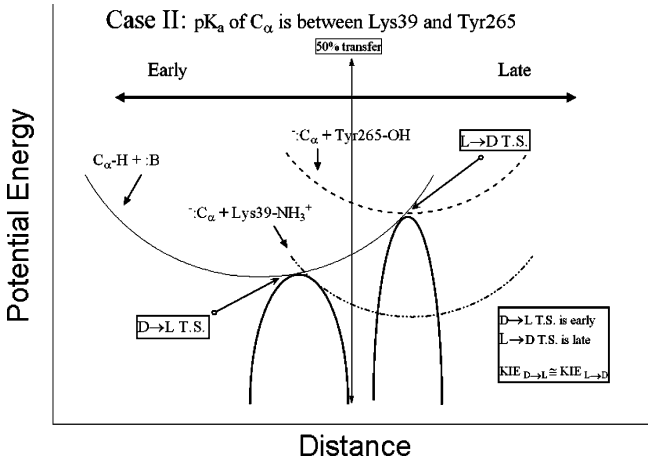

Scheme 5

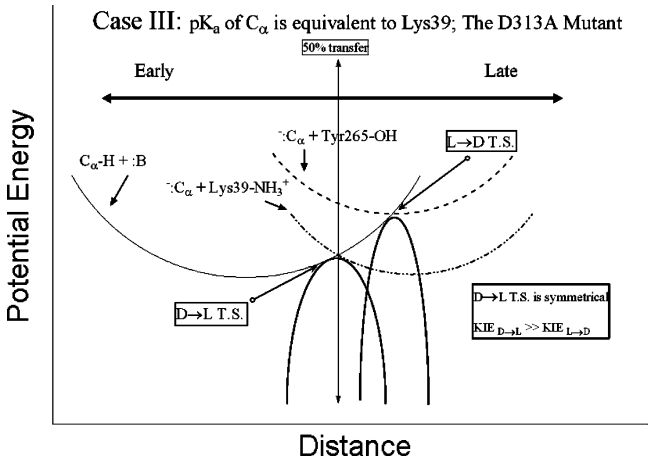

curves approximate the location of the transition state for proton transfer. The dotted line in the center of each scheme indicates the point of 50% proton transfer.

In case I (Scheme 3), the pK_a of the substrate Cα lies above the pK_a values of both K39 and Y265. In this case, one would expect the intrinsic KIE in the D → L direction (where K39 acts as a general base) to be relatively large and larger than (i.e., the transition state more nearly symmetric) that in the L → D direction, since the ΔpK_a between Cα and K39 would be smaller compared to the ΔpK_a between Cα and the phenolic oxygen of Y265. This is not borne out here where the intrinsic KIE in the L → D direction is slightly larger than that in the D → L direction and both are small compared to the theoretical maximum of ∼7.[25]

In case II, the pK_a of the Cα proton lies between those of the two catalytic bases. One expects an early transition state for proton abstraction in the D → L direction (K39 pK_a > Cα pK_a) and a late one in the L → D (Y265 pK_a < Cα pK_a) direction. This situation can potentially give a wide variation in the relative values of the intrinsic KIEs, depending on the relative magnitudes of the ΔpK_a values for Cα and K39 vs Y265 and therefore the location of the proton in the transition states relative to the midpoint.

If the pK_a of the Cα proton lies exactly between the pK_a values of the two catalytic bases, then one would expect the two intrinsic KIEs to be the same, but the transition state in the D → L direction to be *early* and that in the L → D direction to be *late*. If the pK_a of the Cα proton were to lie slightly closer to Y265 than to K39, for instance, if it had a value of approximately 9 (and K39 and Y265 had microscopic pK_a values of ∼11.5 and ∼7.4, respectively), then one would expect the transition state in the D → L direction to be late and the KIE somewhat smaller than in the L → D direction. This is consistent with the intrinsic KIEs and is depicted in Scheme 4 (case II). This likelihood highlights the importance of the reverse protonation state for AlaR in the nonphysiological D → L reaction. The catalytically active reverse protonated form of the external aldimine in the D → L direction is much higher in energy than the typically protonated form (see Figure S2 of the Supporting Information), and the transition state from this high-energy reverse protonated state would be early compared to that for the L → D direction.

One may also consider the formal possibility where the pK_a of Cα is lower than that of either K39 or Y265. Since one would not expect it to be much lower than the pK_a of Y265 in the external aldimine intermediate (∼7.4), the prediction of this case is that the L → D KIE would be large, much larger than for the D → L direction. This is not consistent with the intrinsic KIEs and therefore is discounted as a possibility.

If case II is correct and the pK_a of Cα is between those of K39 and Y265, then selectively lowering the pK_a of K39 would give a more symmetric transition state and a larger KIE in the D → L direction. This scenario is depicted in case III (Scheme 5). Such a mutant (D313A) has been analyzed in our laboratory (unpublished results). The carboxylic oxygen of D313 is 2.8 Å from the ϵ-nitrogen of K39 and probably contributes to the high pK_a of K39 by electrostatically stabilizing the protonated form. The mutant has an additional ionization at 9.3 ± 0.3 (ascribed to K39) in the k_{cat} vs pH profiles that is not present in the wild type, which has only a single ionization with a pK_a of ∼7.4. The D313A mutant also has a large ^DV isotope effect (>3.5) at alkaline pH, with a pK_a of 9.1 ± 0.2 in the pH vs ^DV profile. These results are consistent with proton removal from the high-energy $ED_{reverse}$ external aldimine giving an early transition state and the low pK_a of Y265 giving a late transition state in the L → D direction.

The global analysis performed in this study, which yields the free energy profiles illustrated in Figure 3, does not distinguish between different protonation states of the intermediates (i.e., all possible protonation states are subsumed into a single species). A more complex and more realistic model would allow alanine to form external aldimines in all possible protonation states, which can interconvert. For D-Ala, the reactive, high-energy protonation state **3**, from which Cα proton abstraction would actually take place, would be energetically separated from the three other protonation states in such an analysis. Thus, the ED ground state in Figure 3 should be viewed as a weighted average of the energies of the four possible protonation states.

Free energy calculations by Major and Gao predict a pK_a for Cα−H in AlaR of 12.2.[15] They estimated that the enzyme active site contributes 6.6 kcal/mol to the acidification of Cα−H relative to an aqueous environment.[15] This Cα−H pK_a is higher than suggested by the current study, which would produce a transition state at the interface of cases I and II discussed above.

Secondary KIEs. Schiff base formation is a multistep transimination process encompassing nucleophilic attack of the

unprotonated substrate amino group on the protonated internal aldimine to give a geminal diamine, followed by proton transfer between geminal nitrogens, and finally collapse to the external aldimine intermediate. This multistep process was modeled as a single step in the present analysis. Therefore, the observation of a significant KIE on the single rate constant used to describe the multistep Schiff base formation (and decomposition) process indicates that the rate-limiting elementary step in this multistep process must be collapse of the geminal diamine to the external aldimine, since hyperconjugation of the Cα−H bond with the Schiff base is the most obvious source of a significant secondary KIE in this process and only occurs at this last step. The large intrinsic secondary KIEs suggest that the Cα−H in both external aldimines is close to perpendicular to the plane of the PLP ring, since hyperconjugation is maximal when the Cα−H bond is parallel to the p orbitals of the conjugated Schiff base/pyridine ring π system.

The secondary KIEs obtained in the present analysis (Table 2) are similar to values obtained for solvolytic reactions: 1.15−1.2 in the $sp^3 \rightarrow sp^2$ direction and 0.83−0.87 in the $sp^2 \rightarrow sp^3$ direction, which give EIEs of ∼1.4 for a single deuteron in the isotopically sensitive position.[32] The existence of a secondary EIE is also supported by calculated EIEs presented in Table S5. The particular vibrational frequency calculation employed appears to underestimate the secondary EIE by about 10%, on the basis of test cases for which experimental secondary EIEs are available. A 10% correction would place these calculated EIEs at ∼1.14−1.17, close to the values presented in Table 2.

The large EIEs are evidence for a decreased Cα−H bond order due to strong hyperconjugation with the Schiff base/pyridine ring conjugated π system. This ground-state destabilization of the substrate is likely a major catalytic factor in AlaR (and other PLP enzymes) and is intimately linked to the lowering of the Cα−H pK_a by the combination of the PLP coenzyme and the active site environment. Dunathan pointed out years ago that such bond labilization could be a major determinant of reaction specificity that is enforced simply by binding the substrate such that the appropriate bond is parallel to the p orbitals of the conjugated π system.[33]

Conclusions

Global analysis of AlaR isotopic progress curves allows determination of intrinsic KIEs and EIEs from deuterated and protiated free energy profiles. The magnitudes of the intrinsic primary KIEs, the lower boundary on the energy of the quinonoid intermediate, and the obligate reverse protonation state in the D → L direction suggest that the pK_a of Cα−H in the external aldimine lies between the microscopic pK_a values for the two catalytic bases, such that the proton abstraction transition state is early in the D → L direction and late in the L → D direction. Remarkably, intrinsic secondary KIEs and EIEs are found in both the L → D and D → L directions. These are ascribed to a weakening of the Cα−H bond in the external aldimine intermediate by hyperconjugation with the conjugated π system of the Schiff base/pyridine ring.

Supporting Information Available: Computational procedures, Scheme S1, Tables S1−S6, and Figures S1 and S2. This material is available free of charge via the Internet at http://pubs.acs.org.

JA067643K

(32) Isaacs, N. S. *Physical organic chemistry*, 2nd ed.; Longman Scientific & Technical: Burnt Mill, Harlow, Essex, England; Wiley & Sons: New York, 1995; p xxxiv, 877 pp.

(33) Adams, E.; Mukherjee, K. L.; Dunathan, H. C. *Arch. Biochem. Biophys.* **1974**, *165*, 126−32.